Ferrous Iron Reduction of Superoxide, A Proton-Coupled Electron-Transfer Four-Point Test

Matthew C. F. Wander,*,† James D. Kubicki,‡ Aurora E. Clark,† and Martin A. A. Schoonen§

Department of Chemistry, Washington State University, P.O. Box 644630, Pullman, Washington 99164-4630, Department of Geosciences and the Earth & Environmental Systems Institute, 503 Deike Building, The Pennsylvania State University, University Park, Pennsylvania 16802, and Center for Environmental and Molecular Science (CEMS), Department of Geosciences, 255 Earth and Space Sciences Building, Stony Brook University, Stony Brook, New York 11794-2100

Received: July 31, 2008; Revised Manuscript Received: November 7, 2008

Nelsen's four-point method of separating oxidants and reductants has been tested to evaluate its applicability to proton-coupled electron-transfer reactions. An efficient computational method was developed to determine rate-limiting steps in complex, multistep redox reactions. Geochemical redox reactions are rarely single-step, and by identifying the rate-limiting steps, computational time can be greatly reduced. The reaction of superoxide and ferrous oxide was selected as a test case for its simplicity and its importance in environmental radical generation chemistry (Fenton's reaction). Two approaches, one quantum mechanical and the other semiempirical, were compared. In both approaches, hybrid density functional theory (DFT) was used with the B3LYP/6-31+G(d,p) basis set and a polarized continuum model of the solvent to minimize the structures and determine the energies. In the quantum mechanical case, DFT was used to determine both the Gibbs free energies and the values for the intrinsic component of the reorganization energy of possible combinations of reactants and products. In the latter, experimental ΔG_f values were combined with calculated intrinsic reorganization energy values. The computational results matched the relative difference in rate barriers between the reduction of superoxide by ferrous iron above and below pH 4.8. In the acidic pH range, the proton is coupled to the electron transfer, whereas in the neutral case, the proton initiates the electron transfer.

Introduction

In environmental chemistry, few electron-transfer reactions occur without coupled H^+ transfers. Thus, changes in an atom's oxidation state can lead to changes in pK_a and orbital hybridization, altering a proton's position along the reaction pathway.[1] Examples of environmentally significant proton coupled electron-transfer reactions include O_2 gas reduction, disproportionation of U(V) into U(IV) and U(VI), sulfide oxidation in acid mine drainage, and pyrite oxidation.[2−4] To complicate matters further, many environmental redox processes involve multiple electron-transfer reactions and proceed by more than one reaction path. Proton transfers can occur in conjunction with, prior to, or after electron transfers.[5−9] The multitude of pathways indicates a need for an efficient method of determining relative barrier heights. Computational methods can clarify the complex potential energy surface (PES) by identifying and focusing on the key, rate-limiting steps of the reaction.

This proof-of-concept article illustrates the Marcus theory principle of separability of reactants in a common class of electron-transfer (ET) reactions, specifically those involving proton-coupled electron transfers (PCETs). Marcus theory acts as a framework for single-step reaction paths involving electron transfer. This framework deconstructs the rate into its primary components

$$k_{ET} = \nu_n \exp\left\{\frac{1}{kT}\left[\frac{(\Delta G_{rxn} + \lambda)^2}{4\lambda} - V_{AB}\right]\right\} \quad \text{where } \lambda = \lambda_E + \lambda_I \quad (1)$$

In eq 1, ν_n (the prefactor) is the frequency of the vibrational mode associated with the reaction coordinate in the adiabatic case; k is the Boltzmann constant; T is the temperature in Kelvin; ΔG_{rxn} (Gibbs free energy of ET) is the thermodynamic driving force; V_{AB} (the electronic overlap integral) is the energy of stabilization relative to the diabatic crossing point of the transition state, which results from coupling reactant (donor) and product (acceptor) orbitals; λ_I (the intrinsic component of the reorganization energy) is the energy required to rearrange the nuclei from a reactant to a product configuration while maintaining the electronic state of the reactants and vice versa; and λ_E (the external reorganization energy) is the energy required to rearrange the solvent to accommodate the displaced charge of the electron. This behavior is diagrammed in Figure 1. A large V_{AB} value indicates adiabatic ET, whereas a small value indicates diabatic transfer. Taken together, these components allow for an exact determination of the barrier height. Errors in the calculated rate of reaction depend on the methods employed.

Here, we demonstrate that PCET reactions are further separable in the same way that pure electron-transfer reactions are: reactants and products can be treated independently within the Marcus framework in eq 1. Within this approximation, it is possible to estimate the barrier heights of reaction energies of complex environmental PCET mechanisms using combinations of PCET half-cell reactions. These half-cell reactions incorporate a correction for the proton solvation energy, which is added to

* Corresponding author. E-mail: mwander@wsu.edu.
† Washington State University.
‡ The Pennsylvania State University.
§ Stony Brook University.

10.1021/jp806842f CCC: $40.75 © 2009 American Chemical Society
Published on Web 01/15/2009

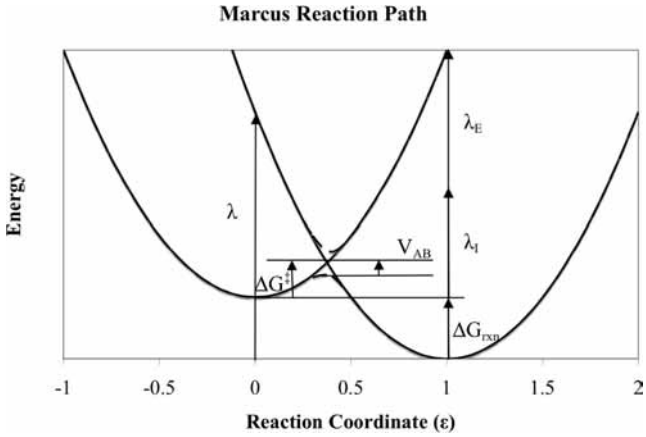

Figure 1. Schematic diagram of a generalized redox reaction showing the important components of the Marcus rate expression within the Marcus−Hush approximation. The magnitude of V_{AB} in this schematic is 5% of λ. Even a V_{AB} of this magnitude would affect the position of the adiabatic minima relative to the diabatic minima,[50] but at this scale, the effect is not apparent.

one half-cell reaction and subtracted from the other, which leads to a cancelation when the half-cell potentials are recombined to determine the relative barrier heights. These estimates can be used to select the most favorable mechanism for a given reaction. This method will reduce the degree of difficulty involved in determining the lowest relative barrier among a class of possible mechanisms, within the uncertainty of the computational approach.

In this article, the PCET extension of Nelsen's four-point method is benchmarked by estimating barrier heights for the reaction between Fe(II) and superoxide at two different pHs and is shown to correctly determine the known lower barrier. The reduction of superoxide by Fe(II)(aq) was chosen for this proof-of-concept study because the reaction rates have been measured experimentally.[10] The overall reaction chemistry changes as a function of pH. For pH < 4.8, the overall reaction is

$$Fe^{2+}(aq) + HOO^{\bullet} + H_2O(aq) \rightarrow Fe(III)OH^{2+}(aq) + H_2O(aq) \quad (2)$$

Above pH 4.8, the dominant reaction is

$$Fe^{2+}(aq) + OO^{-\bullet} + 2H_2O(aq) \rightarrow Fe(III)(OH)_2{}^{+}(aq) + H_2O_2(aq) \quad (3)$$

As can be seen in eqs 2 and 3, the final protonation state of $Fe^{3+}(aq)$ depends on pH. Within the reactants, a direct 1:1 conversion of $HOO^{\bullet}$ to $OO^{-\bullet}$ occurs, so the concentrations of the two can be considered equal.[10] The rate constant for eq 2 is 1.2×10^6 at pH 1, and that for eq 3 is 1.0×10^7 at pH 6. A sharp transition occurs at pH 4.8,[10] indicating that different mechanisms drive eqs 2 and 3. Assuming a rate constant based on eq 1 and using a value of 1.85×10^{13} for ν_n, the experimental values for $\Delta G^{\ddagger}$ are 41.0 ± 0.4 and 35.8 ± 0.3 kJ/mol for eqs 2 and 3, respectively. Considering the similarity of the values, only a qualitative, relative comparison of the differences between experimental and theoretical models can be made.

Theoretical Background: Four-Point Separation Method

In pure electron transfer, it has already been demonstrated that the oxidants and reductants of the reaction can be separated to calculate the electronic reorganization energies, thereby providing an estimate of the reaction barrier.[11] This approach

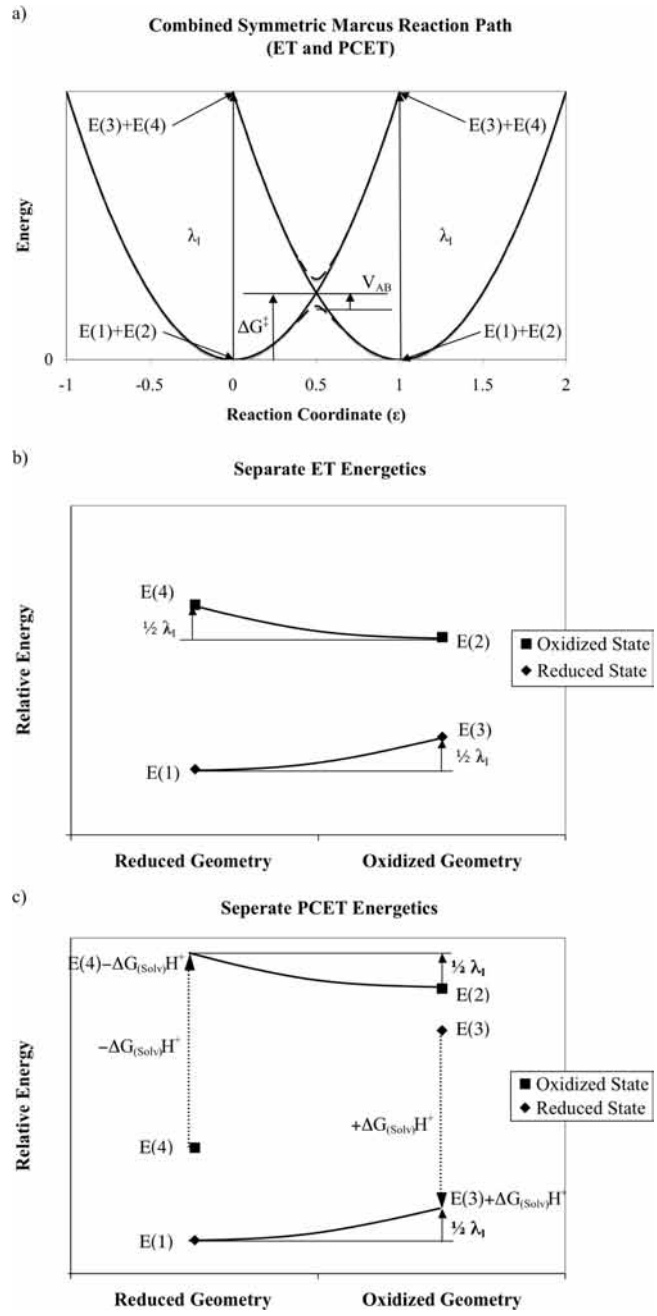

Figure 2. Demonstration of the method for separating reactants from products in an redox reaction for both pure ET and PCET reaction types. Please see the note in the Figure 1 caption regarding the magnitude of V_{AB}. (a) Simplified version of Figure 1, in which the effects of the external reorganization energy and the free energy of reaction have been neglected to focus solely on the separation of intrinsic reorganization energies. (b) Reproduction of Nelsen et al.'s figure demonstrating the separation of the components of the intrinsic barrier height shown in part a. (c) In the same way, these components add to form the barrier in part a, with the proton solvation terms canceling exactly.

has been benchmarked extensively for a wide variety of systems from organic to geochemical.[12−23] In Figure 2b the reactants and products are considered separately as oxidized and reduced end members. As the geometries change along the reaction coordinate, the energies rise quadratically until a charge-reversed state is reached. In the context of separate reactants and products, the charge-reversed state is decomposed into the reduced wave function evaluated at the oxidized geometry and the oxidized wave function evaluated at the reduced geometry. To determine the intrinsic component of the reorganization energy, the

differences between the two states evaluated for the two geometries are averaged.

In the case of the PCET reaction discussed in this work, the half-cell reactions require an additional term that corresponds to the energy generated when a proton is brought to the system from vacuum. It approximates the energy of H^+ in solution and cancels when the total reorganization energy of the reaction is calculated, but is present for separated reactants/products

$$\begin{aligned} &\text{H-donor} \rightarrow \text{donor} + e^-(aq) + H^+(aq) + H^+(aq) \\ &+ e^-(aq) + \text{acceptor} \rightarrow \text{H-acceptor} \\ &= \text{H-donor} \rightarrow \text{H-acceptor} \end{aligned} \quad (4)$$

Both e^- and H^+ have nonzero absolute energy values that contribute to the half-cell reaction thermodynamics. In Figure 2c and a, we show how

$$\lambda_I = [E(3) + E(4)] - [E(1) + E(2)] \quad (5)$$

where 1−4 refer to points in Figure 2a−c and E is just the energy evaluated at the corresponding point. Equation 5 summarizes the fundamental components of the four-point separation method. This is the same as the pure ET case and is not dependent on the energies of e^- and H^+. A similar, semiempirical approach has been developed using ab initio values of the intrinsic reorganization energy and experimental free energies of reaction.[24]

It is well-known that it is impossible to match experimental rate constants by separating reactants from products, as the four-point model ignores two important contributions to the rate: (a) a moving electron rearranges the local water structure, and (b) the donor and acceptor orbitals overlap at the transition state. Both of these are functions of distance between reactants and products in the encounter complex. In a, the reorganization energy of the external solvent (λ_E) is approximated by the Marcus continuum expression, which obeys the distance dependence expressed as[25]

$$\lambda_E = (\Delta e)^2(1/2r_1 + 1/2r_2 - 1/R)(1/d_{op} - 1/d_s) \quad (6)$$

In this equation, Δe is the number of electrons transferred; r_1 and r_2 are radii for the donor and acceptor cavities, respectively; R is the distance between the donor and acceptor; d_{op} is the optical dielectric constant; and d_s is the static dielectric constant. In b, V_{AB} decays exponentially with distance[26]

$$V_{AB} = V^0_{AB} \exp[-\beta(R - R_0)/2] \quad (7)$$

Here, V^0_{AB} is the value of V_{AB} at the optimal separation distance R_0, R is the donor−acceptor distance, and β is a system-specific parameter.

As the reactants and products in the calculation are, in effect, separated by infinite distance, these two components of the rate are impossible to incorporate for a fixed, real distance. The model presented in this work presumes that, when comparing steps of the same mechanism, the encounter complex distance will not change significantly and every barrier will have the same relative error

$$[\text{H−donor}] + [\text{acceptor}] \rightarrow [\text{H−donoracceptor}] \rightarrow [\text{donor−H−acceptor}]_1 \quad (8)$$

$$\rightarrow [\text{donor−H−acceptor}]_2 \quad (9)$$

$$\rightarrow [\text{donor−H−acceptor}]_3 \quad (10)$$

In eqs 8−10, [H−donor] is the protonated electron donor, [H−donoracceptor] is the encounter complex, and [donor−H−acceptor]$_{1-3}$ are the three possible products from the encounter complex connected by three single-step reactions. Errors in differences between barrier heights in the same mechanism should cancel. In the purely hypothetical case of infinite encounter complex separation, the four-point method produces an exact rate, not a rate difference.

Based on this discussion, an outer-sphere complex appears more amenable to a treatment that assumes infinite separation, whereas for an inner-sphere complex, which has a bond between donor and acceptor, the amenability is less intuitive. First and foremost, Marcus theory makes no formal distinction between inner-sphere and outer-sphere reactions; values will change, but the forms of the equations are identical. For both inner- and outer-sphere complexes, eqs 6 and 7 apply, and V_{AB} and λ_E depend solely on the separation between donor and acceptor for chemically similar systems such as those in different encounter complexes within the same mechanism. In an inner-sphere reaction, the donor and acceptor are usually closer together, so the deviation of the calculated rate from the experimental rate is anticipated to be larger than in the outer-sphere case. If one considers two inner-sphere, mechanistic steps for the same reaction, there are strict chemical limits governing how close the donor and acceptor can be, so two different encounter complexes should have the essentially the same separation between donor and acceptor. This implies that the calculated difference between the two barriers should be the same. This is important because it illustrates the nature of the error in applying this approach: to the extent that two encounter complexes differ in their donor−acceptor distances, there will be an error in the application of this approach. These concerns, which have already been addressed for pure ET, apply to both pure ET reactions and PCET reactions.[11]

Another limitation to obtaining experimentally accurate rates lies in the pre-exponential factor, ν_n, in eq 1. Different values have been proposed for ν_n in adiabatic ET. For most transition metals, the longitudinal optical relaxation frequency is appropriate for electron transfer with a value of 1.85×10^{13} s^{-1}.[27,28] This approach to separating reactants from products to determine approximate barrier height differences is applicable only to systems where equivalent concentrations of reactants are being compared.

Error Analysis. The formula for calculating the diabatic crossing point from Marcus theory is[29]

$$\Delta G^{\ddagger} = \frac{1}{4}\lambda(1 + \Delta G_{rxn}/\lambda)^2 \quad (11)$$

where $\Delta G^{\ddagger}$ refers to the diabatic crossing point and the remaining components have the same meaning as in eq 1. However, this could raise an ambiguity, as $\Delta G^{\ddagger}$ can also refer to the transition state in Eyring theory, which is not intended; in no part of this work are Eying theory or its components used. For $\Delta G_{rxn} \gg 0$, the barrier height is approximately that of the free energy of the reaction

$$\Delta(\Delta G^{\ddagger}) = \Delta(\Delta G_{rxn}) \quad (12)$$

where $\Delta(\Delta G^{\ddagger})$ is the error in the free energy of the barrier and $\Delta(\Delta G_{rxn})$ is the error in the calculated free energy of the reaction. For $\Delta G_{rxn} \approx 0$, this reduces to the symmetric case where $\Delta G^{\ddagger} = {}^1/_4\lambda$ and

$$\Delta(\Delta G^{\ddagger}) = \frac{1}{4}\Delta\lambda \quad (13)$$

where $\Delta\lambda$ is the error in calculating the reorganization energy. As ΔG_{rxn} decreases below zero, the crossing of the curve passing through the reactants' geometry and $\Delta G^{\ddagger}$ approaches zero

$$\Delta(\Delta G^{\ddagger}) \approx 0 \quad (14)$$

Therefore, for chemically relevant ΔG_{rxn} values, the magnitude of $\Delta(\Delta G^{\ddagger})$ is approximately $^1/_4\Delta\lambda$ when $\Delta G_{rxn} \leq 0$. Our calculated error for the relative reaction barrier ($\Delta G^{\ddagger}$) is thus approximately one-fourth of the error resulting from uncertainties in the methodology and basis set use when calculating the reorganization energy.

Computational Methods

Unrestricted B3LYP calculations were performed with the 6-31+G(d,p) basis set using the Gaussian 03 quantum chemistry software package.[30−35] The B3LYP hybrid functional contains a mixture of gradient-corrected correlation and exact exchange from Hartree−Fock. The spin state for Fe^{2+} has four unpaired electrons (high-spin) such that $S = 5$ and $m_s = {}^4/_2$. Fe^{3+} has five unpaired electrons (high-spin) with $S = 6$ and $m_s = {}^8/_2$, and the peroxide radicals have one unpaired electron ($S = 2$, $m_s = {}^1/_2$). The polarized continuum model (PCM) was used to approximate the long-range solvent effects with a dielectric constant of 78.39, and the cavity radii were determined using the default UA0 model.[36,37] This model has been benchmarked extensively for a variety of systems and has been shown to improve the calculation of half-cell potentials when used with explicit solvent.[38−40] Frequency calculations were used to incorporate zero-point corrections into the optimized energies for determining the free energy of the reaction.

Following the guidelines of Uudesasma and Tamm's model of short-range solvation, 18 H_2O molecules were placed around each Fe, corresponding to one inner coordination shell with 6 H_2O molecules and a second solvent shell consisting of 12 H_2O molecules.[38] The six coordinating H_2O molecules of aqueous $Fe^{2/3+}$ are bound strongly to the iron. Six H_2O molecules were used to solvate the superoxide/peroxide species. This combination of explicit and implicit solvents has been used to calculate both accurate pK_a and E_h constants in prior studies.[41−44] The effect of pH was taken into account by adjusting the protonation state of each cluster.

The second method for calculating the relative barrier heights is based on a semiempirical approach. The reorganization energies calculated from the four-point method were used in conjunction with standard-state experimental ΔG^0 values to compute barrier heights.[45] This allowed us to focus exclusively on the quality of our predictions as a function of barrier heights.

As a consequence of the shallow potential energy surface of the solvating water molecules and inaccuracies in the DFT integration grid, some species had small negative frequencies. These were $HOO^{\bullet}\cdot(H_2O)_5\cdot H_3O^+$, −13.1679 cm^{-1}; $HOO^{\bullet}\cdot(H_2O)_6$, −17.1506 cm^{-1}; $Fe^{3+}(H_2O)_{18}$, −7.6202 cm^{-1}; and $Fe_2(OH)_2(H_2O)_{16}$, −22.6645 cm^{-1}. However, these energies were not significant when compared to the methodological error.

The mechanistic steps studied were those corresponding to all the reasonable combinations of proton and electron transfers. In the acidic case, corresponding to eq 2, the mechanistic reactions were

$$Fe^{2+} + HOO + H_3O^+ \rightarrow Fe^{3+} + H_2O_2 \quad (r1)$$

$$Fe^{2+} + HOO + H_2O \rightarrow Fe^{3+} + H_2O_2 + OH^- \quad (r2)$$

$$Fe^{2+} + HOO \rightarrow FeOH^{2+} + H_2O_2 \quad (r3)$$

For the neutral case (eq 3), the mechanistic reactions were

$$Fe^{2+} + O_2^- \rightarrow FeOH^+ + HOO \quad (r4a)$$

$$FeOH^+ + HOO \rightarrow FeOH^{2+} + H_2O_2 + OH^- \quad (r4b)$$

$$Fe^{2+} + O_2^- + 2H_2O \rightarrow Fe(OH)_2^+ + H_2O_2 \quad (r5)$$

$$Fe^{2+} + O_2^- + H_2O \rightarrow FeOH^{2+} + HO_2^- \quad (r6)$$

$$Fe^{2+} + O_2^- + H_2O \rightarrow Fe^{3+} + HO_2^- + OH^- \quad (r7)$$

In all cases, the products and reactants had to be present in at least small concentrations to be considered.

TABLE 1: DFT Energies (in Hartrees) of the Hydrated Clusters of Reactants and Products

cluster	ground state[a]	zero point	charge reversed[b]	cluster	ground state[a]	zero point	charge reversed[b]
$Fe(H_2O)_6^{2+}\cdot(H_2O)_{12}$	−2639.612	0.448	−2639.376	$HOO^{\bullet}\cdot(H_2O)_5H_3O^+$	−610.059	0.171	−610.249
$Fe(H_2O)_6^{3+}\cdot(H_2O)_{12}$	−2639.409	0.446	−2639.581	$H_2O_2\cdot(H_2O)_6$	−610.285	0.167	−609.988
$FeOH(H_2O)_5^{+}\cdot(H_2O)_{12}$	−2639.139	0.436	−2638.936	$HOO^{\bullet}\cdot(H_2O)_6$	−609.606	0.158	−609.789
$FeOH(H_2O)_5^{2+}\cdot(H_2O)_{12}$	−2638.969	0.437	−2639.104	$H_2O_2\cdot(H_2O)_5OH^-$	−609.817	0.156	−609.580
$Fe(OH)_2(H_2O)_4\cdot(H_2O)_{12}$	−2638.661	0.422	−2638.477	$OO^{-\bullet}\cdot(H_2O)_6$	−609.184	0.143	−609.278
$Fe(OH)_2(H_2O)_4^{+}\cdot(H_2O)_{12}$	−2638.509	0.422	−2638.623	$HO_2^-\cdot(H_2O)_5OH^-$	−609.326	0.144	−609.136

[a] Final energy of the optimized cluster with the oxidation state shown. [b] Energy of a single-point calculation with a different oxidation state performed at the same geometry; for Fe^{2+}, that would be an Fe^{3+} energy calculation at that Fe^{2+} geometry and vice versa.

TABLE 2: Predicted Electronic Reorganization Energies for Self-Exchange ET and PCET Reactions as Calculated Using the Four-Point Method[a]

	λ (kJ/mol)		λ/kJ/mol
	Pure ET		
(s1) $Fe(H_2O)_6^{2+}\cdot(H_2O)_{12}//Fe^{+3}(H_2O)_6^{2+}\cdot(H_2O)_{12}$	85	(s7) $H_2O_2\cdot(H_2O)_6//HOO^{\bullet}\cdot(H_2O)_5H_3O^+$	141
(s2) $FeOH(H_2O)_5^{+}\cdot(H_2O)_{12}//FeOH(H_2O)_5^{2+}\cdot(H_2O)_{12}$	89	(s8) $H_2O_2\cdot(H_2O)_5OH^-//HOO^{\bullet}\cdot(H_2O)_6$	70
(s3) $Fe(OH)_2(H_2O)_4\cdot(H_2O)_{12}//Fe(OH)_2(H_2O)_4^{+}\cdot(H_2O)_{12}$	93	(s9) $HO_2^-\cdot(H_2O)_5OH^-//OO^{-\bullet}\cdot(H_2O)_6$	126
	ET with 1PT		
(s4) $Fe(H_2O)_6^{2+}\cdot(H_2O)_{12}//FeOH(H_2O)_5^{2+}\cdot(H_2O)_{12}$	133	(s10) $H_2O_2\cdot(H_2O)_6//HOO^{\bullet}\cdot(H_2O)_6$	150
(s5) $FeOH(H_2O)_5^{+}\cdot(H_2O)_{12}//Fe(OH)_2(H_2O)_4^{+}\cdot(H_2O)_{12}$	118	(s11) $H_2O_2\cdot(H_2O)_5OH^-//OO^{-\bullet}\cdot(H_2O)_6$	187
	ET with 2PT		
(s6) $Fe(H_2O)_6^{2+}\cdot(H_2O)_{12}//Fe(OH)_2(H_2O)_4^{+}\cdot(H_2O)_{12}$	161	(s12) $H_2O_2\cdot(H_2O)_6//OO^{-\bullet}\cdot(H_2O)_6$	267

[a] All have the form $\lambda = {}^1/_2[E$(oxidized state evaluated at the reduced geometry) − E(oxidized state evaluated at the oxidized geometry) + E(reduced state evaluated at the oxidized geometry) − E(reduced state evaluated at the reduced geometry)].

TABLE 3: Possible Elementary Steps for the Potential Reactions and Calculated Energies (kJ/mol)

	$\Delta G_{rxn(calc)}$[a]	$\Delta G_{rxn(exp)}$[b]	λ_I	$\Delta G^{\ddagger}_{(ab\text{-}init)}$	$\Delta G^{\ddagger}_{(semi)}$
	Acidic (pH < 4.8)				
(1) $Fe^{2+} + HOO + H_3O^{1+} \rightarrow Fe^{3+} + H_2O_2$	−78	−64	225	24	29
(2) $Fe^{2+} + HOO + H_2O \rightarrow Fe^{3+} + H_2O_2 + OH^-$	−30	2	155	25	40
(3) $Fe^{2+} + HOO \rightarrow FeOH^{2+} + H_2O_2$	−101	−52	283	29	47
	Neutral (pH > 4.8)				
(4a) $Fe^{2+} + O_2^- \rightarrow FeOH^+ + HOO$	140	11	N/A	N/A	N/A
(4b) $FeOH^+ + HOO \rightarrow FeOH^{2+} + H_2O_2 + OH^-$	−107	−23	159	4	28
(5) $Fe^{2+} + O_2^- + 2H_2O \rightarrow Fe(OH)_2^+ + H_2O_2$	−1	−51	428	107	83
(6) $Fe^{2+} + O_2^- + H_2O \rightarrow FeOH^{2+} + HO_2^-$	33	−13	319	97	74
(7) $Fe^{2+} + O_2^- + H_2O \rightarrow Fe^{3+} + HO_2^- + OH^-$	156	18	210	160	44

[a] Calculated reaction energy. [b] Experimental reaction energy.

Results and Discussion

Table 1 summarizes the results of the DFT geometry optimizations, as well as the charge-reversed, single-point calculations. Then, a series of plausible reaction energies were calculated, and the barrier heights compared, for ET and PCET (Table 2). An examination of the relative energies for ET and PCET reveals a distinct pattern within the potential reaction pathways. The average λ value is 101 kJ/mol (84−140 kJ/mol) for ET, 148 kJ/mol (117−187 kJ/mol) for a single-proton PCET, and 214 kJ/mol (161−266 kJ/mol) for a double PCET. Peroxide reorganization energies were higher than their Fe counterparts, which caused an overlap in the relative energy ranges. Both the peroxide and Fe species showed the same pattern of reorganization energies as a function of proton count. Although not applicable to all PCET reactions or any associated hybridization change, these estimates are useful indicators of one- and two-electron H^+-coupled reactions.

The reorganization energies are composed of a sum of a large positive number [charge-reversed energy minus $\Delta G_{solv}(H^+)$] and a large negative number [charge-reversed energy plus $\Delta G_{solv}(H^+)$], which reflects the loss of H^+ to the individual cluster energy. Overall, the reorganization energies for the reactions are reasonable, for self-exchange reaction s4, in Table 2, column 1:

$$Fe^{2+} + H_2O \rightarrow FeOH^{2+} + H^+ + e^- \qquad (16)$$

and for the full self-exchange reaction

$$\lambda_I = [1334.3\ \text{kJ/mol} + (-1069.3\ \text{kJ/mol})]/2 = 133\ \text{kJ/mol} \qquad (17)$$

The value of energy calculated for λ_I in the half-cell cases is approximately equal to the λ_I for pure ET on an equivalent system, plus the energy associated with protonation of the appropriate group ($\sim\Delta E_{solv}$ for the proton, −1098 kJ/mol), e.g.[46]

$$FeOH(OH_2)_5^{+} + H^+(aq) \rightarrow Fe(OH_2)_6^{2+} \qquad (18)$$

Only the lowest calculated $\Delta G^{\ddagger}$ value for each pH condition can be correlated to the experimental pattern. To benchmark this approach successfully, we require that the lowest neutral $\Delta G^{\ddagger}$ value be lower than the lowest $\Delta G^{\ddagger}$ value predicted for the acidic cases, because the experimental reaction is faster. Reaction r1, in the acidic case, violates these assumptions; the result of the decreased concentration of H^+ with increased pH. Within the pH range 2−4.8, basic stoichiometry is sufficient to tell us that this reaction will be slow compared to reactions r2 and r3. We have no experimental data below pH 2, so the mechanism in that pH range is ambiguous. At some pH below pH 2, reaction r1 should dominate due to increasing H^+ concentration.

In the results for acidic conditions, pH < 4.8 (Table 3), all three predicted ΔG_{rxn} values match the experimental values, within the computational method error of 10−30 kJ/mol.[39] In Table 3, all values are components of or calculated from eq 11. These are the only values that are possible to calculate given the assumptions in this paper. The incorporation of zero-point corrections changes the predicted energies slightly, by ∼5−10 kJ/mol for reaction energies, and ∼1−3 kJ/mol for $\Delta G^{\ddagger}$. In the acidic case, all three mechanisms, reactions 1−3 in Table 3, indicate a proton coupled electron transfer. OOH^- is too thermodynamically unfavorable under acidic conditions to be a reasonable intermediate product, since the deprotonation reaction has $\Delta G_{pK_a} \gg 0$. The reason why mechanism r2 is the fastest is because of its low reorganization energy.

One mechanism dominates in the neutral pH region, as confirmed by quantum mechanical and semiempirical approaches. We predict that the rate-controlling step will be the second reaction (reaction r4b), represented by reactions r4a and r4b. Reaction r4a is the proton-transfer reaction that initiates a subsequent electron transfer. To determine the overall rate for reaction r6, the equilibrium must be included in the rate expression. Because reaction r4a is not favored energetically, the pre-equilibrium approximation is $k_4 = K_{4a}k_{4b}$.[47] Although proton transfer is unfavored, it will occur in small enough quantities to stimulate the second step ($K_{eq} = 0.012$). However, it will raise the barrier from 4 to 15 kJ/mol in the ab initio calculation and from 28 to 39 kJ/mol in the semiempirical calculations.

Our results from the computational work in the neutral case do not correlate as closely with the experimental data as our results for acidic conditions. Specifically, an incorrect value for ΔG_{rxn} of the ferrous iron−superoxide reaction affects the predicted rate in mechanism r4a/b, as the proton transfer occurs before the electron transfer. This type of error has been observed previously in the calculation of pK_a constants using hybrid DFT, and the causes in that work are likely to coincide with the results here.[48] As a result, the semiempirical approach works better and is recommended for those systems with available thermodynamic data.

Quantum mechanical and semiempirical approaches predict the same limiting barrier in each case. The reactions to compare are the ones with favorable ΔG values that have the lowest overall barrier for each category, acidic and neutral. These are reaction 2 (pH < 4.8) and reactions 4a/b (pH > 4.8). The activation energies are 25 kJ/mol (40 kJ/mol semiempirical) and 15 kJ/mol (39 kJ/mol semiempirical), confirming that the neutral pH reaction is faster.

The four-point method simplifies what would otherwise be a complex set of quantum mechanical calculations. Although a complete description is beyond the scope of this work, it requires combining oxidants and reductants together in the same calculation, optimizing the encounter complex and products in the same spin configuration, mapping the reaction path, examining for proton-coupled and -separated pathways for PCET reactions, etc.[49] Separating reactants from products reduces the size and complexity of the calculation to only one redox-active element per cluster. The presence of only one redox-active element means that each calculation is more computationally consistent, assuming that the correct spin states are selected. This system is much less complex than optimizations involving multiple transition metal centers. For a large, complex mechanism, only a handful of reactants need to be calculated rather than reactants and products in combination for every reaction.

Conclusions

In conclusion, when comparing similar reaction types, it is possible to determine the relative reaction rate of concerted proton−electron transfers using the PCET application of Nelsen's four-point method.[11] The separation principle that he described is not altered by the addition of a mobile proton. The proton has been shown to assist the electron transfer for the reaction studied. In the acidic case, all three mechanisms, reactions 1−3 in Table 3, indicate a proton-coupled electron transfer. OOH^- is too thermodynamically unfavorable under acidic conditions to be a reasonable intermediate product, given that the deprotonation reaction has $\Delta G_{pK_a} \gg 0$. In the neutral case, reaction 4a/b in Table 3 is the dominant pathway by which the electron is preceded by the proton. In the future, finding computational approaches to reduce uncertainties in pK_a energy errors will be essential to improving the overall potential of these types of calculations.

Acknowledgment. We would like to acknowlege Karenann Jurecki and Roger Crawford.

References and Notes

(1) Mayer, J. M. *Annu. Rev. Phys. Chem.* **2004**, *55*, 363.
(2) Petlicki, J.; Ven, T. G. M. *J. Chem. Soc., Faraday Trans.* **1998**, *94*, 2763.
(3) Newton, T. W.; Baker, F. B. *Inorg. Chem.* **1965**, *4*, 1166.
(4) Rickard, D.; Luther, G. W. *Geochim. Cosmochim. Acta* **1997**, *61*, 135.
(5) Cukier, R. I.; Nocera, D. G. *Annu. Rev. Phys. Chem.* **1998**, *49*, 337.
(6) Cukier, R. I. *J. Phys. Chem.* **1994**, *98*, 2377.
(7) Cukier, R. I. *J. Phys. Chem.* **1995**, *99*, 16101.
(8) Cukier, R. I. *J. Phys. Chem.* **1996**, *100*, 15428.
(9) Zhao, X. G.; Cukier, R. I. *J. Phys. Chem.* **1995**, *99*, 945.
(10) Rush, J. D.; Bielski, B. H. J. *J. Phys. Chem.* **1985**, *89*, 5062.
(11) Nelsen, S. F.; Blackstock, S. C.; Kim, Y. *J. Am. Chem. Soc.* **1987**, *109*, 677.
(12) Vektaris, G.; Vektariene, A. *Lith. J. Phys.* **2007**, *47*, 15.
(13) Rosso, K. M.; Smith, D. M. A.; Dupuis, M. *J. Chem. Phys.* **2003**, *118*, 6455.
(14) Ma, S. H.; Xu, H.; Zhang, R. B.; Qu, Z. W.; Zhang, X. K.; Zhang, Q. Y. *Acta Chim. Sin.* **2001**, *59*, 2042.
(15) Kelterer, A. M.; Landgraf, S.; Grampp, G. *Spectrochim. Acta A: Mol. Biomol. Spectrosc.* **2001**, *57*, 1959.
(16) Ma, S. H.; Zhang, X. D.; Xu, H.; Shen, L. L.; Zhang, X. K.; Zhang, Q. Y. *J. Photochem. Photobiol. A: Chem.* **2001**, *139*, 97.
(17) Zhang, X. D.; Wang, Y. N.; Guo, J. X.; Zhang, Q. Y. *J. Photochem. Photobiol. A: Chem.* **1999**, *121*, 1.
(18) Guo, J. X.; Zhang, Q. Y. *J. Photochem. Photobiol. A: Chem.* **1997**, *110*, 247.
(19) Lambert, C.; Noll, G. *J. Am. Chem. Soc.* **1999**, *121*, 8434.
(20) Sigman, M. E.; Closs, G. L. *J. Phys. Chem.* **1991**, *95*, 5012.
(21) Finckh, P.; Heitele, H.; Volk, M.; Michelbeyerle, M. E. *J. Phys. Chem.* **1988**, *92*, 6584.
(22) Nelsen, S. F.; Weaver, M. N.; Luo, Y.; Pladziewicz, J. R.; Ausman, L.; Jentzsch, T. L.; O'Konneck, J. J. *J. Phys. Chem. A* **2006**, *110*, 11665.
(23) Nelsen, S. F. Electron transfer reactions within σ- and π-bridged nitrogen-centered intervalence radical ions. In *Advances in Physical Organic Chemistry*; Richard, J. P., Ed.; Academic Press Ltd: London, 2006; Vol. 41; pp 183−216.
(24) Wahlgren, U.; Tsushima, S.; Grenthe, I. *J. Phys. Chem. A* **2006**, *110*, 9025.
(25) Marcus, R. A. *J. Chem. Phys.* **1956**, *24*, 966.
(26) Newton, M. D.; Sutin, N. *Annu. Rev. Phys. Chem.* **1984**, *35*, 437.
(27) Farmer, V. *Mineral. Soc., London* **1974**,
(28) Tsuda, N.; Nasu, K.; Fujimori, A.; Siratori, K. *Electronic Condition in Oxides*, 2nd ed.; Springer-Verlag: Heidelberg, Germany, 2000.
(29) Cannon, R. D. *Electron Transfer Reactions*; Butterworths: London, 1980.
(30) Stevens, P. J.; Devlin, F. J.; Chabalowski, C. F.; Frisch, M. J. *J. Phys. Chem.* **1994**, *98*, 11623.
(31) Becke, A. D. *J. Chem. Phys.* **1993**, *98*, 5648.
(32) Lee, C.; Parr, R. G.; Yang, W. *Phys. Rev. B* **1988**, *37*, 785.
(33) Hehre, W. J.; Ditchfield, R.; Pople, J. A. *J. Chem. Phys.* **1972**, *56*, 2257.
(34) Hariharan, P. C.; Pople, J. A. *Theor. Chim. Acta* **1973**, *28*, 213.
(35) Windus, T. L. *J. Chem. Phys.* **1998**, *109*, 1223.
(36) Cances, E.; Mennucci, B.; Tomasi, J. *J. Chem. Phys.* **1997**, *107*, 3032.
(37) Mennucci, B.; Tomasi, J.; Cammi, R.; Cheeseman, J. R.; Frisch, M. J.; Devlin, F. J.; Gabriel, S.; Stephens, P. J. *J. Phys. Chem. A* **2002**, *106*, 6102.
(38) Uudsemaa, M.; Tamm, T. *J. Phys. Chem. A* **2003**, *107*, 9997.
(39) Foresman, J. B.; Frisch, A. *Exploring Chemistry with Electronic Structure Methods*, 2nd ed.; Gaussian, Inc.: Pittsburgh, PA, 1996.
(40) Foresman, J. B.; Keith, T. A.; Wiberg, K. B.; Snoonian, J.; Frisch, M. J. *J. Phys. Chem.* **1996**, *100*, 16098.
(41) Richardson, W. H.; Peng, C.; Bashford, D.; Noodleman, L.; Case, D. A. *Int. J. Quantum Chem.* **1997**, *61*, 207.
(42) Li, J.; Fisher, C. L.; Chen, J. L.; Bashford, D.; Noodleman, L. *Inorg. Chem.* **1996**, *35*, 4694.
(43) Mouesca, J. M.; Chen, J. L.; Noodleman, L.; Bashford, D.; Case, D. A. *J. Am. Chem. Soc.* **1994**, *116*, 11898.
(44) Chen, J. L.; Noodleman, L.; Case, D. A.; Bashford, D. *J. Phys. Chem.* **1994**, *98*, 11059.
(45) Wahlgren, U.; Tsushima, S.; Grenthe, I. *J. Phys. Chem. A* **2006**, *110*, 9025.
(46) Zhan, C. G.; Dixon, D. A. *J. Phys. Chem. A* **2002**, *106*, 9737.
(47) Rae, M.; Berberan-Santos, M. N. *J. Chem. Educ.* **2004**, *81*, 436.
(48) Klamt, A.; Eckert, F.; Diedenhofen, M.; Beck, M. E. *J. Phys. Chem. A* **2003**, *107*, 9380.
(49) Wander, M. C. F.; Kerisit, S.; Rosso, K. M.; Schoonen, M. A. A. *J. Phys. Chem. A* **2006**, *110*, 9691.
(50) Nelsen, S. F. *Chem.—Eur. J.* **2000**, *6*, 581.

JP806842F